Available online at www.sciencedirect.com
SCIENCE DIRECT®
Control Engineering Practice 13 (2005) 279–289
CONTROL ENGINEERING PRACTICE
www.elsevier.com/locate/conengprac

A hybrid control strategy for active vibration isolation with electrohydraulic actuators

Y. Zhang[a], A.G. Alleyne[b,*], D. Zheng[c]

[a] Innovation Center, Eaton Corporation, 26201 Northwestern Highway, Southfield, MI 48076, USA
[b] Department of Mechanical and Industrial Engineering, University of Illinois at Urbana-Champaign, 1206 W. Green St., Urbana, IL 61801, USA
[c] Mechanical Dynamics Laboratory, General Electric Company, Building K1, Rm 2A2SE, P.O. Box 8, Schenectady, NY 12301, USA

Received 30 August 2002; accepted 9 March 2004

Abstract

This paper presents a hybrid control approach to circumvent the basic trade-off between performance and robustness from an individual controller. This hybrid control strategy utilizes a robust controller for guaranteed robustness when the plant model is not well known, and employs an adaptive controller for high performance after sufficient plant information has been collected. To avoid a degraded transient after controller switching, a bumpless transfer scheme is designed and incorporated into this hybrid control approach. This bumpless transfer design is an extension from a conventional latent tracking bumpless transfer design for a single-input single-output (SISO) plant with 1 degree of freedom (DOF) controllers to either a SISO plant with multiple DOF controllers or a multi-input multi-output (MIMO) plant. Experimental results implemented on an active vibration isolation testbed demonstrate the effectiveness of the proposed hybrid control strategy.

Keywords: Electrohydraulic systems; Adaptive control; Robust control; Switching algorithms; Active control; Vibration isolation

1. Introduction

Active vibration isolation is a natural evolution of passive vibration isolation. The historical development of theoretical concepts necessary for the design of isolation systems was reviewed by Karnopp (1995) while focusing on a relatively simple idea, the skyhook damper, and its applications to seismic isolation platforms and automotive active and semi-active suspensions. There have been several papers published within the active vibration isolation field and many different control methods have been utilized. Interested readers can refer to Hrovat (1997) and Housner et al. (1997) for surveys of control methods utilized previously.

It is well known that adaptive control and robust control are two popular approaches for the control of uncertain systems. However, either approach has its own advantages and disadvantages. For example, an adaptive controller can achieve high performance for a slowly time-varying or time-invariant uncertain plant after parameter estimation convergence, but it is possible to exhibit poor transient response when the adaptation is initiated. Another disadvantage of adaptive control is that it is sensitive to unmodeled dynamics and disturbances (Ioannou & Kokotovic, 1984). On the other hand, a well-designed robust controller can guarantee robust stability of the closed-loop system under a reasonable class of disturbances and system uncertainties. However, robust controller design is usually conservative because the controller is often based on a worst-case scenario and thus sacrifices part of the achievable performance to guarantee system robustness (Song, Longman, & Mukherjee, 1999). In this work, we propose an alternative hybrid control strategy that switches between a robust controller and an adaptive controller to achieve both controllers' merits and avoid having to choose between either performance or robustness.

When considering switching between controllers, a common problem encountered is the degraded switching transient. One remedy for this is to incorporate a smoothing algorithm to facilitate the transition between

*Corresponding author. Truck Technology Eaton Corporation, 26201 Northwestern Highway, Southfield 48076, USA. Tel.: +1-248-226-6365; fax: +1-248-226-6818.
E-mail addresses: yishengzhang@eaton.com (Y. Zhang), alleyne@uiuc.edu (A.G. Alleyne), zheng@crd.ge.com (D. Zheng).

0967-0661/$ - see front matter © 2004 Elsevier Ltd. All rights reserved.
doi:10.1016/j.conengprac.2004.03.009

controllers. This type of a process is called Bumpless Transfer, which is defined as the transfer, or switch, between one controller acting in closed loop on a plant and a second controller waiting to take over. Bumpless transfer is often formulated into a tracking problem and the tracking algorithms use an input–output setup to let the second controller track the first one while the first one is active and the second is waiting. The interested reader can examine the work by Edwards and Postlethwaite (1998) where different schemes were compared; additional references can also be found in Zheng and Alleyne (2003). A conventional bumpless transfer design was proposed by Graebe and Ahlen (1996), but its application is limited to a single-input single-output (SISO) plant with 1 degree of freedom (DOF) controllers. An extension is made in the current work to make this latent tracking design also suitable to either a SISO plant with multiple DOF controllers or a multi-input multi-output (MIMO) plant. Experimental results demonstrate the effectiveness of the proposed hybrid control approach including the bumpless transfer design.

The rest of this paper is formulated as follows. In Section 2, the vibration isolation problem will be formulated as a position-tracking problem, which is an improved version of the velocity-tracking approach proposed in Zhang and Alleyne (2001). Section 3 introduces a plant model along with the experimental testbed on which the subsequent controller design methods will be presented. In Section 4, an MRAC controller is designed and Section 5 illustrates an H_∞ controller design. The hybrid control approach is presented in Section 6. Section 7 details a new bumpless transfer design and incorporates it into the hybrid control approach, which is followed by experimental results demonstrating the effectiveness of the overall hybrid control strategy. A conclusion then summarizes the main points and contributions.

2. Problem formulation

The types of isolation systems under consideration here are specifically those that are relatively large, requiring high power actuation with a significant bandwidth. The potential applications include active suspensions, seismic isolation, or shock and vibration isolation for land and sea vehicles. Based on the speed and power requirements, electronically controlled hydraulics, or electrohydraulics, will be the focus of the work presented here. Previous work (Zhang & Alleyne, 2003) contains detailed motivations for the current problem formulation to be outlined below and the reader is referred there for additional background information on the problem under study. This motivation is based on an explanation of inherent system limitations with electrohydraulic actuators for most other vibration isolation problem formulations. In the current paper, a basic single DOF active vibration isolation case shown in Fig. 1 will be studied for focused exposition. However, the insight presented here are applicable to multiple DOF cases.

It has been shown that the inertial or "skyhook" damper illustrated in Fig. 2 can achieve very good overall vibration isolation characteristics (Karnopp, Crosby, & Harwood, 1974). Although it is not possible to find a physical inertial reference to place the skyhook damper in most real applications, it is appropriate to choose a skyhook damper system as the reference system for the real plant in Fig. 1 to emulate. The transfer function relationship from the disturbance position to the absolute position of the isolated mass in Fig. 2 is

$$\frac{x_{des}(s)}{z(s)} = \frac{\omega_n^2}{s^2 + 2\zeta\omega_n s + \omega_n^2}. \tag{1}$$

The natural frequency and damping ratio in Eq. (1) are $\zeta = b/2\sqrt{Mk}$ and $\omega_n = \sqrt{k/M}$, respectively, and they can be tuned to achieve some desired response.

In most active vibration isolation problems, the measurement of the disturbance acceleration is more feasible than that of the disturbance position. The acceleration measurement can be performed by placing an accelerometer on the base in Fig. 1. Similarly, it is

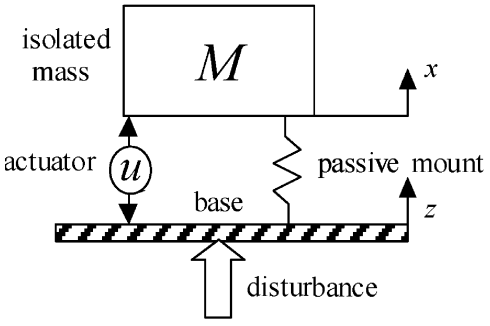

Fig. 1. Disturbance rejection schematic.

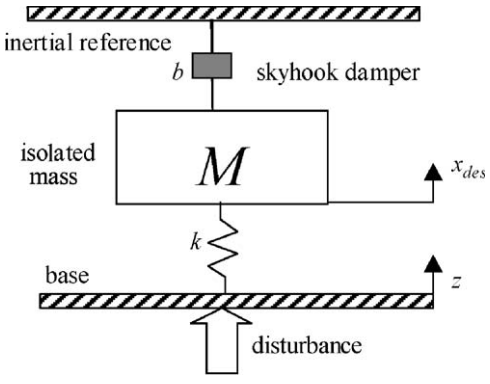

Fig. 2. Skyhook damper representation.

difficult to measure the absolute position of the isolated mass but relatively easy to measure its relative position $(x-z)$ as shown in Fig. 1. Correspondingly, the more useful transfer function relationship between the disturbance acceleration and the relative position of the isolated mass $x_{ref}(\equiv x_{des}-z)$ in Fig. 2 can now be written as

$$G_{ref}(s)=\frac{x_{ref}}{\ddot{z}}=\frac{x_{des}-z}{z}\frac{1}{s^2}=-\frac{s+2\zeta\omega_n}{s(s^2+2\zeta\omega_n s+\omega_n^2)}. \quad (2)$$

In order to avoid possible drift in the reference position x_{ref} due to biased acceleration measurement and the integrator in Eq. (2), a bandpass filter can be utilized to take care of the drift problem and clear high frequency noise in the measured acceleration signal before it goes through the transfer function as shown in Eq. (2).

If the overall objective for the real plant in Fig. 1 is to achieve skyhook damping, the actuator must force the transfer function relationship from the disturbance acceleration to the relative position of the isolated mass to be the same as Eq. (2). Therefore, the active vibration control problem can be formulated as a position-tracking control problem depicted in Fig. 3. The relative position x_{ref} of the isolated mass in a system with a skyhook damper could then be used as the reference command to a feedback control loop.

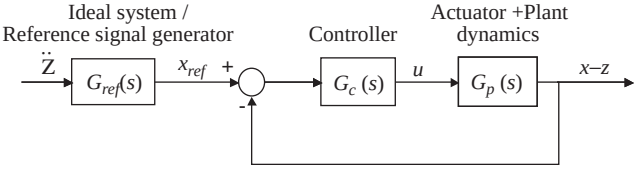

Fig. 3. Position-tracking approach framework.

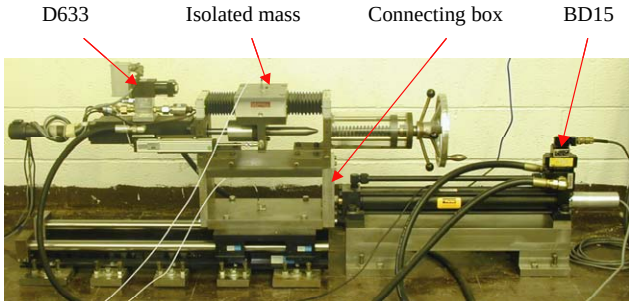

Fig. 4. Active vibration isolation testbed.

3. Experimental testbed and plant model

An active vibration isolation testbed constructed at UIUC is shown in Fig. 4. The vibration isolation subsystem consists of an isolated mass, a Moog direct drive proportional control valve D633, and an electro-hydraulic Moog double-rod cylinder actuator that sits on a connecting box. The connecting box, which travels along a linear bearing system, is attached to a Parker Hannifin hydraulic cylinder controlled by a BD15 electrohydraulic servo valve. The Parker cylinder works as the disturbance generator. This system is a horizontal analog to the system shown in Fig. 1, which makes it an adequate platform to test the active vibration isolation schemes under consideration. The open-loop transfer function of the plant for two experiments at each of two different input voltage levels is given in Fig. 5.

The frequency responses are very reproducible from one experiment to the next but they do show variation with respect to the input amplitude. The reason for this is that the valve's analog electronics impose a rate limit on the valve itself and the overall system also has time-varying characteristics. For the purpose of this investigation, the nominal system transfer function from the Moog D633 valve control input to the Moog cylinder position is identified as

$$G_p(s)=\frac{4775}{s(s^2+464s+119360)}\frac{m}{V}, \quad (3)$$

where the amplifier gain and sensor gain are included.

4. Model reference adaptive controller design

Electrohydraulic systems often exhibit time-varying and nonlinear characteristics. The system dynamics change with respect to oil temperature, supply pressure, etc. Therefore, a Model Reference Adaptive Control

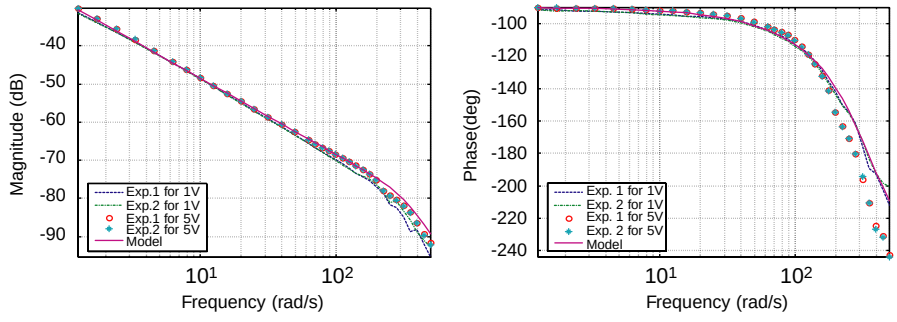

Fig. 5. Experimental and modeled frequency responses of control actuator.

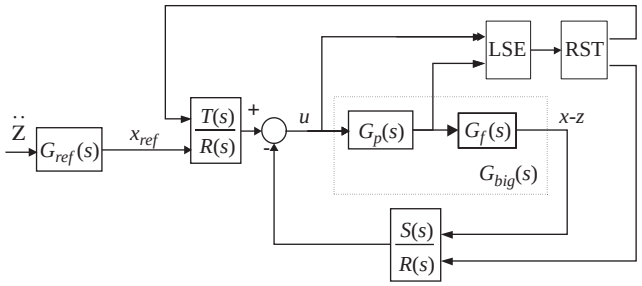

Fig. 6. MRAC framework.

(MRAC) design, which consists of on-line parameter estimation and Model Reference Control (MRC), is selected to implement the position-tracking approach. MRC is a method by which desired closed-loop characteristics can be introduced into a system, i.e. a pole placement method. It consists of a feedforward term $T(s)/R(s)$ and a feedback term $S(s)/R(s)$. The idea behind the controller is to cancel out the unwanted plant dynamics and replace them with the designer's own desired dynamics. MRAC has a systematic method for the controller design and interested readers can refer to Astrom and Wittenmark (1995) for the classic formulation of the MRAC.

The MRAC framework shown in Fig. 6 consists of a feedforward term $T(s)/R(s)$, a feedback term $S(s)/R(s)$, a least-squares estimator (LSE) block, a controller calculation block RST which solves the Diophantine Equation on-line, and a filter $G_f(s)$ which filters LVDT measurement noise for feedback, etc. This is an indirect adaptive control approach where the controller parameters are continuously updated from the identified plant parameters. The LSE is developed in a continuous-time framework with a forgetting factor:

$$\dot{\hat{\theta}} = P(t)\phi(t)e(t), \tag{4}$$

$$\mathrm{e}(t) = y(t) - \phi^{\mathrm{T}}(t)\hat{\theta}, \tag{5}$$

$$\dot{P}(t) = \alpha P(t) - P(t)\phi(t)\phi^{\mathrm{T}}(t)P(t), \tag{6}$$

where $e(t)$ is the identification error, $y(t)$ is the plant output, $\phi(t)$ is the regressor vector, $\hat{\theta}(t)$ is the estimated parameter vector, $P(t)$ is the covariance matrix, and α is the forgetting factor.

From the identified system model, the estimated plant transfer function from control input to actuator position output has the following structure:

$$G_p(s) = \frac{b}{s(s^2 + a_1 s + a_2)}\frac{m}{V}, \tag{7}$$

where a_1, a_2, and b are unknown parameters and $\hat{\theta} = [\hat{a}_1\ \hat{a}_2\ \hat{b}]^{\mathrm{T}}$. The free integrator in $G_p(s)$ is regarded as a known dynamics and is omitted in the adaptation to simplify the LSE block. The filter $G_f(s)$ has the following transfer function:

$$G_f(s) = \frac{300}{s + 300}. \tag{8}$$

In order to be accurate, this filter is included in the overall open-loop plant, $G_{big}(s)$ in Fig. 6, for solving the Diophantine equation.

Choosing a desired model is a very critical issue for MRAC design. Generally speaking, a high bandwidth of the desired model will give good tracking results. Unfortunately, if the desired bandwidth is set too high, this allows unwanted high-frequency noise to enter the feedback loop and deteriorate system performance. Therefore, the reference model should be chosen with a bandwidth higher than the expected disturbance bandwidth yet low enough to avoid sensor noise problems. The BD15 Parker–Hannifin servo valve of the electrohydraulic disturbance generator is limited to a bandwidth of 20 Hz. Therefore, 20 Hz is chosen as the maximum disturbance frequency that will be input to the system. Since the overall open-loop plant $G_{big}(s)$ has a relative degree of 4, the desired model should have a relative degree no less than 4. After some design iterations, the desired model was chosen as

$$G_m(s) = \frac{1.350e11\ (s + 1.6)\ (s + 100)}{(s^2 + 1000s + 3.725e5)\ (s^2 + 800s + 3.625e5)\ (s + 1)\ (s + 160)}. \tag{9}$$

The bandwidth of this desired model is 32 Hz according to the -45° phase condition.

Experiments demonstrate that parameter estimation works well and the parameter convergence process is similar to that shown in Zhang and Alleyne (2001). Defining $\omega_n = 10\pi$ and $\zeta = 1.0$ for $G_{ref}(s)$, the corresponding experimental results are shown later in Fig. 8. The "Theoretical II" in Fig. 8 designates the analytical acceleration RMS ratio for an ideal skyhook damper system. Here, acceleration RMS ratio is defined as $\|$isolated mass acceleration$\|_2/\|$disturbance acceleration$\|_2$ for some fixed time window. The control results from the MRAC match those of a theoretical skyhook damper very closely at lower frequencies, but deteriorate at higher frequencies due to the control system performance roll-off. As an aside, the performance of the current position-tracking approach is superior to previous work using a velocity-tracking approach (Zhang & Alleyne, 2001) due to the reduced effects of sensor noise when using position feedback vs. velocity estimation.

While the isolation performance demonstrated by the MRAC is very good after parameter convergence, the transient performance during the convergence is quite poor. This results from the basic MRC strategy being very sensitive to model uncertainty due to the pole placement strategy. We require an alternate control design method that will give some level of tracking

performance with a guarantee of stability for the uncertainty levels present in the system. This robust controller can be switched into the feedback loop when the adaptive controller is not performing well. Consequently, an H_∞ controller is designed to handle the uncertainty in parameters and still provide some level of performance.

5. H_∞ Controller design

A typical H_∞ control schematic is illustrated in Fig. 7(a). G represents the open-loop interconnection, which contains all of the known information such as nominal plant model, performance, and uncertainty weighting functions. G has three sets of inputs: perturbation input w, disturbance d, and control signal u. Correspondingly, three sets of outputs are generated by G: perturbation output z, error e, and measurement y. K is the feedback controller. The model perturbation $\|\Delta\|_\infty < 1$ is used to characterize the model inaccuracy and the fictitious perturbation $\|\Delta_p\|_\infty < 1$ is used to characterize performance requirements.

Before resorting to any toolbox for numerical solutions, the open-loop interconnection G has to be constructed and its weighting matrices have to be chosen. The construction of G involves generalizing the plant inputs and outputs into standard $[w\ d\ u]^{\mathrm{T}}$ and $[z\ e\ y]^{\mathrm{T}}$ in Fig. 7(a), and selecting appropriate weighting functions to represent performance specifications, noise properties, disturbances, and model perturbation properties. The open-loop interconnection in Fig. 7(b) is constructed for the H_∞ controller design. d_1, d_2, d_3 and d_4 represent LVDT measurement noise, disturbance from the interaction between the isolated mass and the bearing system upon which it is supported, disturbance acceleration, and acceleration measurement noise, respectively. The signals e_1 and e_2 represent weighted control input and weighted tracking error, respectively. u is the control input and y_1 and y_2 are the measurements of isolated mass relative position and disturbance acceleration, respectively. According to the identified characteristics of the testbed, the disturbance

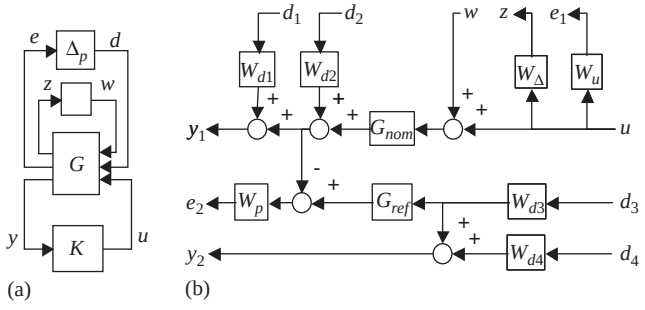

Fig. 7. H_∞ control design.

weighting functions are chosen to have the following characteristics:

$$W_{d_1}(s) = \frac{5e-4(2s+5)}{s+600}, \tag{10}$$

$$W_{d_2}(s) = 2e-4, \tag{11}$$

$$W_{d_3}(s) = \frac{(s+5)\ (s+600)}{(s+25)\ (s+120)}, \tag{12}$$

$$W_{d_4}(s) = \frac{(s/3+1)\ (s/1000+1)}{(s+1)\ (s/3000+1)}. \tag{13}$$

The control input weighting function is defined in Eq. (14) to make the control input less than 5 V, which is the saturation limit of the amplifier for the Moog Direct Drive Valve.

$$W_u(s) = 0.2. \tag{14}$$

The tracking error weighting function is set as

$$W_p(s) = 40\,\frac{s+1}{(s/150+1)^4}. \tag{15}$$

W_Δ is the plant multiplicative uncertainty function:

$$W_\Delta(s) = \frac{s/600+0.1}{s/1200+1}, \tag{16}$$

where the plant is assumed to have 10% uncertainty at DC and 200% uncertainty in the high-frequency range. G_{nom} is the nominal plant model and has the following transfer function:

$$G_{nom}(s) = \frac{4775}{(s+1e-5)\ (s^2+464s+119360)}. \tag{17}$$

The free integrator in Eq. (3) is approximated by $1/(s+1e-5)$ in Eq. (17) with the aim of avoiding numerical computation problem specific to MATLAB μ-tools. The reference system is revised as

$$G_{ref}(s) = -\frac{s+2\zeta w_n}{(s+2)\ (s^2+2\zeta w_n s+w_n^2)}. \tag{18}$$

The free integrator in Eq. (2) is replaced by $1/(s+2)$ in Eq. (18) and this comes from the trade-off between achievable performance and numerical computation specific to MATLAB μ-tools. $\omega_n = 10\pi$ and $\zeta = 1.0$ are used here to be consistent with the previous MRAC results. Based on this design plant model, a sub-optimal H_∞ controller is designed using MATLAB μ-tools, achieving a maximum μ value at 0.994 which means robust performance can be guaranteed.

The experimental results obtained by using this sub-optimal H_∞ controller are shown in Fig. 8, where "Theoretical I" denotes the analytical ratios from the revised reference system in Eq. (18) and "Theoretical II" represents the analytical ratios from the original reference system in Eq. (2).

Experimental results show the H_∞ controller design achieves adequate vibration abatement. However, the

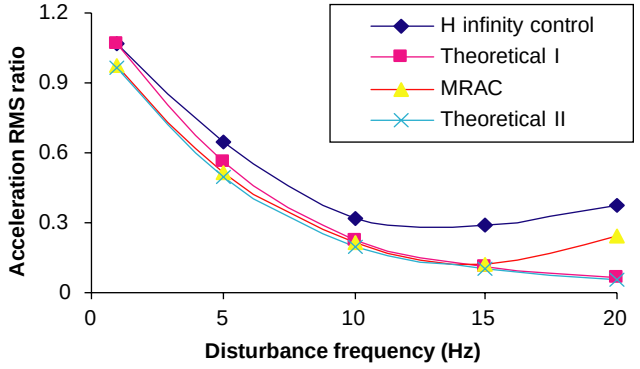

Fig. 8. Performance of MRAC and H_∞ controllers.

acceleration RMS ratios of the H_∞ controller are larger than those of the MRAC controller. This is a result of a less-accurate tracking performance at higher frequency disturbances for the H_∞ controller. The advantage of the H_∞ controller design is that it guarantees robust stability of the closed-loop system throughout the range of conditions expected in implementation, whereas the MRAC controller during large initial parameter estimation errors would perform significantly worse than the H_∞. The different control results presented in Fig. 8 are a result of the different goals of these two controller designs. The H_∞ controller design considers both performance and robustness at the same time. It is thus conservative by sacrificing part of achievable performance to ensure robustness while the MRAC design targets for performance alone while not taking robustness into account.

6. Hybrid control approach

In the presence of uncertainty or varying plant parameters, controller design methodologies based on a single controller are often unable to provide both performance and robustness. This point is demonstrated by the above MRAC and H_∞ controller designs in Sections 4 and 5. It should be noted here that for the purpose of the approach to be presented shortly, many different types of control techniques could have been used instead of the chosen two as long as one was focused primarily on robust stability and the other focused on tracking performance. One approach to circumvent the inherent limitation of a single controller is to use multiple controllers designed to provide either high performance or robustness, as well as intelligent mechanisms to orchestrate the switching among them. The theoretical basis for this approach is provided in the field of Switching Control. This field has seen a steady development over the past decade with several fundamental issues being both framed and explored (Morse, Mayne, & Goodwin, 1992; Morse, 1996; Kulkarni & Ramadge, 1996; Hespanha & Morse, 1999). Recent developments regarding stability and design of Switching Control are surveyed in Liberzon and Morse (1999).

From the results in Sections 4 and 5, the MRAC and H_∞ control designs are found to be effective control methods with regard to system performance and robustness, respectively. It is desirable to realize the strengths of both control designs in one control system while avoiding their shortcomings. The approach being proposed here is a hybrid control approach that switches between the MRAC and H_∞ controllers depending on the different focus on performance or robustness at different times and working conditions. As mentioned earlier, the hybrid control approach presented below is extendable to any hybrid control approach that contains an adaptive controller focused on tracking performance and one another type of fixed robust controller.

6.1. Switching design

The hybrid control strategy schematic is depicted in Fig. 9. The LSE block is used in both the Decision Maker and the MRAC controller. Therefore, this block runs continuously, even when the current active controller is not the MRAC controller. The identification error $e(t)$ from the LSE block gives some indication of the extent of plant identification information that has been collected on-line and the achievable tracking performance of the adaptive controller. This indication is effective when either the H_∞ or MRAC controller is active. Because the identification error $e(t)$ may pass through zero during parameter estimation, a window of error data is used. The windowing period, t_p, also determines the interval between two consecutive decision-making actions, and any switching action can happen only at the end of a windowing period. The flow chart of the decision-making is depicted in Fig. 10(a). The signal $e_{\max}(t)$ has the following nonlinear relationship with the identification error $e(t)$:

$$e_{\max}(t) \equiv \|e(t)\|_\infty \quad t \in ((k-1)t_p, \quad kt_p], \tag{19}$$

where $k \in [1, 2, 3, \ldots]$. Following this equation, $e_{\max}(kt_p)$ will assume the maximum absolute value of the

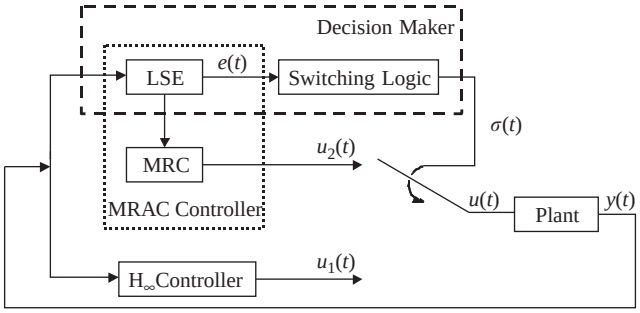

Fig. 9. Designed hybrid control approach schematic.

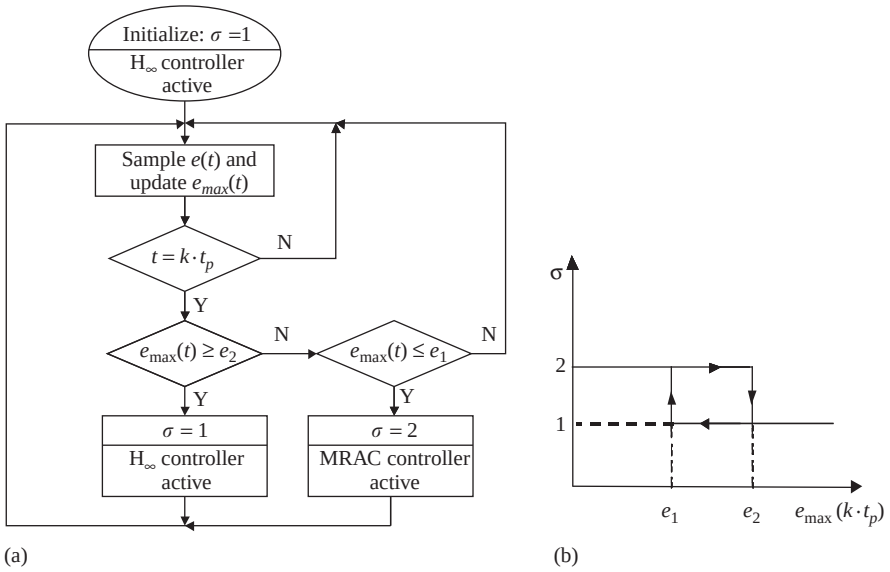

Fig. 10. Design of switching mechanisms.

identification error $e(t)$ during the kth windowing period. Therefore $e_{\max}(kt_p)$ indicates the overall plant identification information that has been collected on-line and the overall achievable tracking performance of the adaptive controller during the kth windowing period. It is thus reasonable to use $e_{\max}(kt_p)$ to decide switching actions.

Switching operations are fulfilled by comparing the error signal $e_{\max}(kt_p)$ to two preset error limits, e_1 and e_2. If $e_{\max}(kt_p) < e_1$, it can be assumed that sufficient plant information has been collected by the LSE and the adaptive controller is able to achieve high performance if it is active. Therefore, the adaptive controller will be active for the next windowing period. If $e_{\max}(kt_p) > e_2$, it means that the LSE has not identified the plant parameters well enough and good performance cannot be guaranteed by the adaptive controller. Therefore, the H_∞ controller will be active for the next windowing period. If $e_{\max}(kt_p)$ is between e_1 and e_2, the active controller in the past windowing period will be kept active for the next windowing period to prevent frequent switching. The hysteresis relation between $e_{\max}(kt_p)$ and the switching variable σ is further illustrated in Fig. 10(b).

Remark. In some sense, the above switching scheme is similar to the dead-zone technique, which is frequently used to make the estimator robust for some adaptive control systems. One example of the dead-zone technique (Slotine & Li, 1991) is illustrated in Eq. (20).

$$\dot{\hat{a}} = \begin{cases} -\gamma v e & |e| > \Delta \\ 0 & |e| < \Delta, \end{cases} \tag{20}$$

where $\hat{a}$ is the estimated parameter, e is the estimation error, and Δ is the size of the dead-zone. When the estimation error is within the small limit Δ, the adaptation mechanism is shut off to avoid parameter drift and instability. However, there exist key differences between the dead-zone technique of Eq. (20) and the current switching scheme. For the dead-zone technique, the control structure with the adaptation mechanism on or off is the same. The dead-zone technique is trying to make only the estimator robust. For the switching scheme presented here, the adaptation mechanism is continuously active. The control structure before and after the switching is different since different controllers are utilized. The switching scheme is trying to make the controller/estimator pair robust.

An appropriate choice for the time window in Eq. (19) is very important in the overall controller design. The windowing period t_p can be chosen by the following equation:

$$t_p = 0.5\frac{1}{f}, \tag{21}$$

where f represents the lowest frequency component expected in the disturbance signals. Note that the zero frequency component in disturbance signals, if it exists, is not within our interest because usually it does not need to be abated. Therefore, it should be omitted when determining f. The reason for using 0.5 in Eq. (21) is that only the absolute value of the identification error $e(t)$ is considered for determining a corresponding $e_{\max}(kt_p)$. This t_p selection can usually preclude the possibility of chatter and provide enough time for the switching transient to decay. Too short a windowing period t_p may lead to wrong switching actions because the corresponding $e_{\max}(kt_p)$ in Eq. (19) may not indicate the overall achievable tracking performance of the adaptive controller fairly. On the other hand, too long

a windowing period t_p could degrade the effectiveness of the switching control because the switching may happen far later than it should. Because poor transient performance from the adaptive controller may damage the plant, a safe experimental way to set the parameters e_1 is to run a stand-alone test with the system controlled by the H_∞ controller. The decision-maker block works in parallel to record the time history of $e_{\max}(t)$. Assuming t_1 is the time instant when the estimated parameters reach steady states, the parameter e_1 can be chosen as the corresponding $e_{\max}(kt_p)$ with $t_1 \in ((k-1)t_p, kt_p]$. The parameter e_2 can then be set as $(1.5 \sim 2)\ e_1$ to prevent frequent switching.

6.2. Switching stability

Stability of a switched system can usually be ensured by keeping each stabilizing controller in the loop for a sufficiently long time so that the transient effects can dissipate. Slow switching assumptions can greatly simplify the stability analysis and are, in one form or another, ubiquitous in the switching control literature (Liberzon & Morse, 1999). Hespanha and Morse (1999) proved that switching among stable linear systems results in a stable system provided that switching is "slow-on-the-average", i.e., the average dwell time between controller switchings is no shorter than a finite time constant, which depends on system matrices. For the current hybrid control strategy, the windowing period t_p and the hysteresis relation shown in Fig. 10(b) can both be utilized to prevent infinitely fast switching and provide time for the switching transient to decay. For many real plants, only one switchover from the H_∞ controller to the MRAC controller is needed if using the proposed hybrid control strategy. In this case, the stability will not become an issue because the transient effect from the switching has enough time to dissipate by assuming that the MRAC controller can always stabilize the plant after the switching. A more general case would include jumps in plant parameters which may result in a finite number of switchovers between these two controllers. In this case, the stability can be guaranteed under the assumption that both the H_∞ controller and the MRAC controller can stabilize the plant. For the case of an infinite number of switchings, which could result from periodic jumps in plant parameters, the stability can still be achieved by setting the windowing period t_p sufficiently long, in addition to the assumption that both controllers are exponentially stabilizing with a certain stability margin.

For the experimental results shown later, the value of t_p is chosen as 0.5 s, which is one half of the period of the lowest interested frequency: defined here as 1 Hz. A low-pass filter with a cut-off frequency of 100 Hz is used to filter the noise from the identification error $e(t)$. From experiments, the value of e_1 and e_2 are set as $2.0e-5$ and $3.5e-5$, respectively. Fig. 11 shows some experimental results using the hybrid control approach to reject a 10 Hz sinusoidal disturbance input. The H_∞ controller is active before 19.5 s and the MRAC controller takes over after that time instant. Fig. 11(a) shows the performance improvement after the switching at 19.5 s. However, there is a degraded transient after the switching. The reason for this is the abrupt jump in control input shown in Fig. 11(b). This abrupt jump comes from a discontinuity in the controllers being used to control the plant. One remedy for this is to incorporate a smoothing algorithm, or bumpless transfer, to facilitate the transition between controllers.

7. Bumpless transfer design

7.1. SISO design

To avoid the unwanted switching transient mentioned in Section 6, a new bumpless transfer design is conducted here. The idea is to make one controller active and then let the other controller follow the active controller with a latent tracking loop so that it can smoothly take over the previous active controller if switching happens. The approach to be followed here is

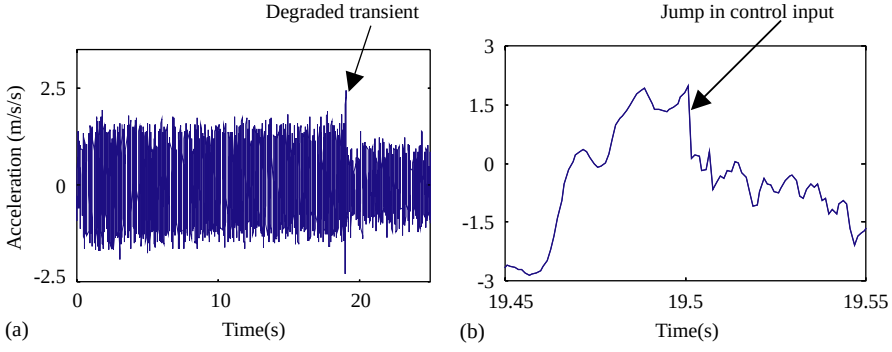

Fig. 11. Experimental results using hybrid control approach.

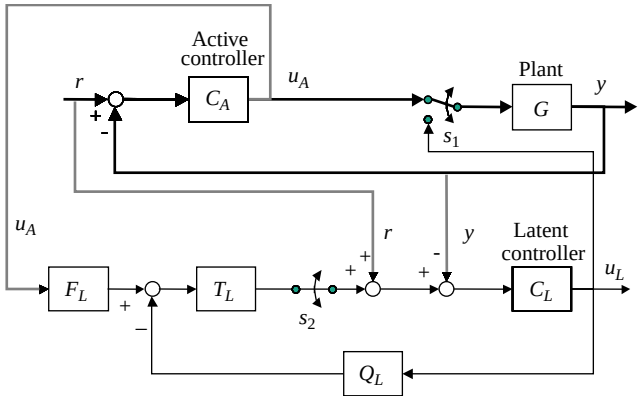

Fig. 12. Unidirectional bumpless transfer diagram.

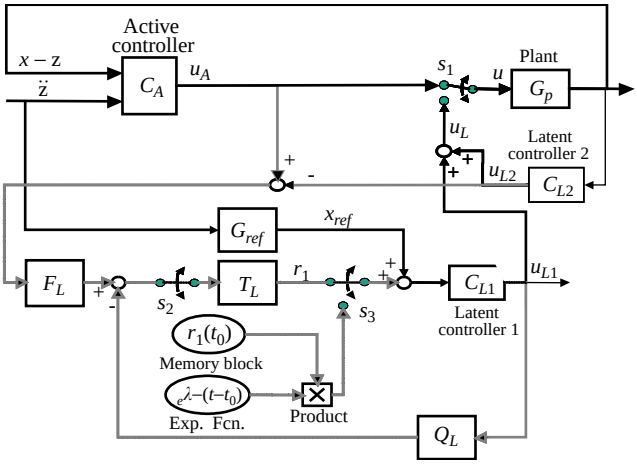

Fig. 13. Bumpless transfer strategy with reference conditioning.

similar to Graebe and Ahlen (1996) where they propose a latent tracking scheme with detailed analysis and design procedures.

Fig. 12 is a general framework in which the problem of bumpless transfer is recast into a tracking problem. G denotes the transfer function of a SISO plant currently controlled by the active controller C_A and the active closed loop depicted by the bold lines in Fig. 12 has the following transfer function relationship:

$$y = \frac{C_A G}{1 + C_A G} r. \tag{22}$$

An additional feedback configuration shown by the regular lines in Fig. 12 has the following transfer function:

$$u_L = \frac{F_L T_L C_L}{1 + T_L C_L Q_L} u_A + \frac{C_L}{1 + T_L C_L Q_L}(r - y), \tag{23}$$

which describes the two DOF tracking loop of the lower part of Fig. 12. The latent controller C_L takes the role of a dynamical system whose output u_L is forced to track the active control signal u_A which acts as the reference signal to the tracking loop. Since the latent tracking loop takes into account the reference signal r and plant output y as disturbance generators, it will cause the output u_L of the second controller to asymptotically track the output u_A of the first controller. The convergence of the controller tracking is based on the design of the tracking controller triplet (F_L, T_L, and Q_L). Assuming the tracking transient has decayed, the outputs of the active and latent controllers should be identical at the time of controller switching: t_0. Since the control signal received by the plant will be identical before and after t_0, the transients associated with the switch should be minimized. After t_0, the previously active controller C_A is disconnected and the previously latent controller C_L then works as the current active controller $\forall t > t_0$.

$$y = \frac{C_L G}{1 + C_L G} r. \tag{24}$$

If the latent tracking loop is disconnected right after the switching, the previously latent and currently active controller C_L in Fig. 12 will initiate its own output trajectory immediately. This sudden change in latent tracking input will introduce another unwanted transient. One remedy is to use a reference conditioning method to "recondition" the reference of the controller C_L. In this case, the modified reference will allow the controller C_L to eliminate the influence of the latent tracking and converge to its own trajectory gradually and smoothly. The approach used here is shown in the bottom part of Fig. 13. The reference conditioning design includes a switch s_3, a memory block with constant $r_1(t_0)$ and an exponentially decaying function $e^{-\lambda(t-t_0)}$. The constant $r_1(t_0)$ represents the output of the T_L block at the time instant of the switching operation t_0. Switch s_2 will be open and switch s_3 will be closed at t_0. Then the exponentially decaying function $e^{-\lambda(t-t_0)}$ will cause a dynamical decay of $r_1(t_0)$ to zero. This decayed signal is added onto the current active controller input and works as a smoothing function. There exists some trade-off to choose an appropriate value for the λ in the exponentially decaying function $e^{-\lambda(t-t_0)}$. Usually, λ can be set such as the time constant of the exponentially decaying function $e^{-\lambda(t-t_0)}$ is between $(0.2 \sim 0.4)t_p$.

7.2. H_∞–MRAC bumpless transfer

The above bumpless transfer scheme is for a SISO plant with 1 DOF controllers. It can be extended to more general cases such as a SISO plant with multiple DOF controllers or a MIMO plant. For any SISO plant, usually one latent tracking loop is sufficient for unidirectional bumpless transfer no matter how many DOFs the controllers may have. For any MIMO system, one latent tracking loop is often sufficient for each plant input and thus the number of overall necessary latent tracking loops in the whole system is equal to the

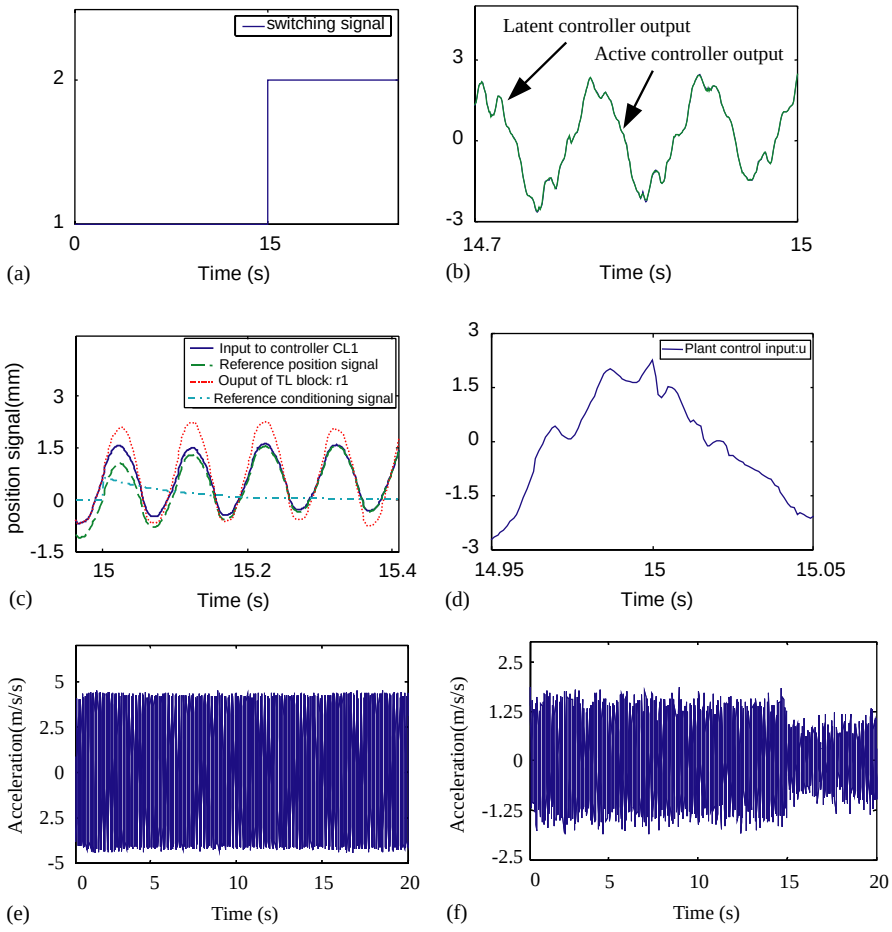

Fig. 14. Experimental results of hybrid control approach with bumpless transfer design.

number of the plant inputs. For bidirectional bumpless transfer, the number of necessary latent tracking loops will be doubled.

For graphical clarity, only unidirectional bumpless transfer design corresponding to the switching from the H_∞ controller to the MRAC controller is depicted in Fig. 13. However, the procedure is easily extendible to bidirectional transfers. The active controller C_A represents the designed H_∞ controller with two inputs, disturbance acceleration $\ddot{z}$ and plant relative position output $x-z$, and one output u_A. The MRAC controller is comprised of the feedforward controller C_{L1} with input x_{ref} and output u_{L1}, as well as the feedback controller C_{L2} with input $x-z$ and output u_{L2}. G_p represents the controlled plant and the currently active closed loop is depicted by the bold lines. The regular solid lines constitute the MRAC control loop and the dotted lines are for the purpose of latent tracking. The latent tracking loop forces the output u_{L1} of the latent controller C_{L1} to track u_A-u_{L2}, which is the active controller output u_A minus the output u_{L2} of the latent controller C_{L2}. According to the following relationship:

$$u_{L1}=u_A-u_{L2}\Leftrightarrow u_L=u_{L1}+u_{L2}=u_A, \tag{25}$$

a smoothed plant control input, u, can be achieved after switching if the latent tracking loop performs well.

Experimental evaluation is carried out after incorporating the bumpless transfer design into the hybrid control approach described in Section 6. The tracking controller triplet has the following settings: $F_L=Q_L=1$, $T_L=20$. The constant λ in the exponentially decaying function $e^{-\lambda(t-t_0)}$ is set as 10 so that it will give a time constant of about 0.2 s, which is 40% of the windowing period t_p in the previous hybrid control design.

Fig. 14 shows the experimental results using the hybrid control approach including the extended bumpless transfer design. The disturbance is a 10 Hz sinusoidal signal. Fig. 14(a) indicates that the H_∞ controller is active before 15 s and the MRAC controller takes over after that time. The effectiveness of the bumpless transfer design is demonstrated in Fig. 14(b), where the "Latent controller output" and "Active controller output" represent u_L and u_A, respectively. Fig. 14(c) illustrates the input to the latent controller C_{L1} which switches from the T_L block output r_1 to the reference position signal x_{ref} smoothly because of the added reference conditioning. Fig. 14(d) demonstrates that the smoothed transition of this input signal avoids

the abrupt jump in plant control input u as shown in Fig. 11(b). Compared to the time history of the disturbance acceleration in Fig. 14(e), Fig. 14(f) shows satisfactory acceleration reduction under the H_∞ controller at the beginning of the experiment and significantly improved performance under the MRAC controller after the switching. The experimental results demonstrate the potential of the proposed hybrid active vibration isolation system to achieve better performance while maintaining a high degree of robustness.

8. Conclusion and discussions

Design of a hybrid strategy for robust and high-performance vibration control is presented. This strategy is designed to combine the merits of adaptive control and robust control while circumventing inherent trade-off between performance and robustness from either of them. The resulting hybrid controller is more flexible and versatile than either adaptive control or robust control alone. A new bumpless transfer design, which is an extension of a conventional latent tracking bumpless transfer design for a SISO plant with one DOF controllers to either a SISO plant with multiple DOF controllers or a MIMO plant, is conducted to avoid a degraded transient after controller switching. Experimental results demonstrate the effectiveness of the hybrid control strategy with the bumpless transfer design incorporated.

Acknowledgements

The authors are very grateful to Professor Daniel Liberzon of the University of Illinois for illuminating discussions on the hybrid control strategy reported on this article.

References

Astrom, K. J., & Wittenmark, B. (1995). *Adaptive Control* (2nd ed). Reading MA: Addison-Wesley Publishing Company, Inc.

Edwards, C., & Postlethwaite, I. (1998). Anti-windup and bumpless-transfer schemes. *Automatica*, *34*(2), 199–210.

Graebe, S. F., & Ahlen, A. (1996). Dynamic transfer among alternative controllers and its relation to antiwindup controller design. *IEEE Transactions on Control Systems Technology*, *4*(1), 92–99.

Hespanha, J. P., & Morse, A. S. (1999). Stability of switched systems with average dwell-time. *Proceedings of the 38th Conference on Decision and Control*, pp. 2655–2660.

Housner, G. W., Bergman, L. A., Caughey, T. K., Chassiakos, A. G., Claus, R. O., Masri, S. F., Skelton, R. E., Soong, T. T., Spencer, B. F., & Yao, J. T. P. (1997). Structural control: past, present, and future. *Journal of Engineering Mechanics*, *123*(9), 897–971.

Hrovat, D. (1997). Survey of advanced suspension developments and related optimal control applications. *Automatica*, *33*(10), 1781–1817.

Ioannou, P. A., & Kokotovic, P. V. (1984). Instability analysis and improvement of robustness of adaptive systems. *Automatica*, *20*(5), 583–594.

Karnopp, D. (1995). Active and semi-active vibration isolation. *Journal of Mechanical Design*, *117B*, 177–185.

Karnopp, D., Crosby, M. J., & Harwood, R. A. (1974). Vibration control using semi-active force generators. *Journal of Engineering for Industry*, *96*(2), 619–626.

Kulkarni, S. R., & Ramadge, P. J. (1996). Model and controller selection policies based on output prediction errors. *IEEE Transactions on Automatic Control*, *41*(11), 1594–1604.

Liberzon, D., & Morse, A. S. (1999). Basic problems in stability and design of switched systems. *IEEE Control Systems Magazine*, *19*(5), 59–70.

Morse, A. S. (1996). Supervisory control of families of linear set-point controllers—Part I: exact matching. *IEEE Transactions on Automatic Control*, *41*(10), 1413–1431.

Morse, A. S., Mayne, D. Q., & Goodwin, G. C. (1992). Applications of hysteresis switching in parameter adaptive control. *IEEE Transactions on Automatic Control*, *37*(9), 1343–1354.

Slotine, J., & Li, W. (1991). *Applied nonlinear control*. Englewood Cliffs, NJ: Prentice-Hall.

Song, G., Longman, R. W., & Mukherjee, R. (1999). Integrated sliding-mode adaptive-robust control. *IEE Proceeding: Control Theory and Applications*, *146*(4), 341–347.

Zhang, Y., & Alleyne, A. (2001). A novel approach to active vibration isolation with electrohydraulic actuators. *Proceedings of the 2001 ASME IMECE*, New York, USA.

Zhang, Y., & Alleyne, A. (2003). A simple novel approach to active vibration isolation with electrohydraulic actuators. *ASME Journal of Dynamic Systems, Measurement, and Control*, *125*, 125–128.

Zheng, D., & Alleyne, A. (2003). Modeling and control of an electrohydraulic injection molding machine with smoothed fill-to-pack transition. *ASME Journals of Manufacturing Science and Technology*, *125*, 154–163.